

# Study of the eightfold degeneracy with a standard $\beta$ -Beam and a Super-Beam facility

A. Donini<sup>a</sup>, E. Fernandez-Martinez<sup>a</sup>, P. Migliozzi<sup>b</sup>, S. Rigolin<sup>a</sup> and L. Scotto Lavina<sup>c</sup>

<sup>a</sup> I.F.T. and Dep. Física Teórica, U.A.M., E-28049, Madrid, Spain

<sup>b</sup> I.N.F.N., Sezione di Napoli, I-80126, Napoli, Italy

<sup>c</sup> Dip. Fisica, Università di Napoli "Federico II" and I.N.F.N., I-80126, Napoli, Italy

## Abstract

The study of the eightfold degeneracy at a neutrino complex that includes a standard  $\beta$ -Beam and a Super-Beam facility is presented for the first time in this paper. The scenario where the neutrinos are sent toward a Megaton water Cerenkov detector located at the Fréjus laboratory (baseline 130 Km) is exploited. The performance in terms of sensitivity for measuring the continuous ( $\theta_{13}$  and  $\delta$ ) and discrete ( $\text{sign}[\Delta m_{23}^2]$  and  $\text{sign}[\tan(2\theta_{23})]$ ) oscillation parameters for the  $\beta$ -Beam and Super-Beam alone, and for their combination has been studied. A brief review of the present uncertainties on the neutrino and antineutrino cross-sections is also reported and their impact on the discovery potential discussed.

# 1 Introduction

In the past years the hypothesis of neutrino oscillations has been strongly confirmed in the atmospheric [1], accelerator [2], solar [3] and reactor [4] sectors. If we do not consider the claimed evidence from the LSND experiment [5], that must be confirmed or excluded by the ongoing MiniBooNE experiment [6], oscillations in the leptonic sector can be accommodated in the three family Pontecorvo-Maki-Nakagawa-Sakata (PMNS) mixing matrix [7]. Therefore, the next steps on the way of a full understanding of neutrino oscillations are:

- confirm the source of atmospheric neutrino oscillations, i. e. observe directly the  $\nu_\mu \rightarrow \nu_\tau$  oscillation;
- perform precision measurements of the angles  $\theta_{12}$  and  $\theta_{23}$  and of the mass differences  $|\Delta m_{12}^2|$  and  $|\Delta m_{23}^2|$ ;
- measure the sign of the atmospheric mass difference,  $\Delta m_{23}^2$ ;
- measure the remaining parameters of the PMNS mixing matrix:  $\theta_{13}$  (for which only an upper limit exists so far [8]) and the leptonic CP violating phase  $\delta$  (that is still completely unknown).

With the aim to perform the above measurements, over recent years there has been a marked growth of interest in the development of new neutrino sources: conventional neutrino beams from pion and kaon decay, but with a more intense flux (Super-Beams); neutrino beams from muon decays (Neutrino Factories); neutrino beams from the decay of intense beams of  $\beta$ -unstable heavy ions ( $\beta$ -Beams). For a comprehensive review of future neutrino sources we refer to [9] and references therein.

In this paper we focus on a CERN-based neutrino complex including a  $\beta$ -Beam, that could leverage existing facilities at CERN and complement the EURISOL physics program [10], and a Super-Beam based on an intense proton driver (the SPL). Although the possibility to exploit higher  $\gamma$   $\beta$ -Beams has been put forward (see for example [11, 12]), we consider here only the configuration of the  $\beta$ -Beam where  $\nu_e$  ( $\bar{\nu}_e$ ) are produced by  $^{18}\text{Ne}$  ( $^6\text{He}$ ) ions [13] that are accelerated by the SPS up to  $\gamma \sim 100$  ( $\gamma \sim 60$ ), respectively (standard  $\beta$ -Beam). These  $\gamma$  values have been chosen in order to tune the neutrino/antineutrino mean energy in such a way that the maximum of the atmospheric neutrino oscillation lies at a distance of around 100 Km, i.e the distance from CERN to Fréjus.

A first estimate of the potentiality of a CERN to Fréjus based neutrino complex was given in Ref. [13]. However, in that study only the intrinsic degeneracy<sup>1</sup> was taken into account and only the very peculiar value  $\delta = 90^\circ$  was considered. In Ref. [11] a

---

<sup>1</sup>i.e. the sign of the atmospheric mass difference  $\Delta m_{23}^2$  is assumed to be positive and  $\theta_{23} = 45^\circ$ .

more thoughtful analysis, on both experimental and theoretical issues, appears even if again only positive  $\Delta m_{23}^2$  and  $\theta_{23} = 45^\circ$  were considered, the main interest of the paper being the study of higher  $\gamma$  setups.

The Super-Beam envisaged at the CERN neutrino complex studied in this paper is based on the planned SPL of 4 MW power described in Ref. [14]. Similar projects have been also proposed in Japan and USA, and carefully studied by several authors [15], with neutrinos energies around 1-2 GeV. The Super-Beam studied in this paper has an average neutrino energy around 0.25 GeV to match the CERN-Fréjus distance. A comprehensive analysis of the CERN-based Super-Beam potential, although based on old fluxes and considering only the intrinsic degeneracy, can be found in [14].

In this paper we study for the first time the complete eightfold degeneracy for the CERN neutrino complex, i.e. the  $\beta$ -Beam and the Super-Beam either separately or together. In Section 2, the neutrino oscillation formalism is introduced and the eightfold degeneracy discussed from a theoretical point of view. The main features of the neutrino complex at CERN are discussed in Section 3, while the set of cross-sections used in this paper are briefly summarized in Section 4. In particular, we compared these cross-sections with other calculations and briefly comment the present status of the cross-section knowledge for neutrino energies below 1 GeV. Finally we give our results on the sensitivity calculation both for the  $\theta_{13}$  angle and the CP violating phase  $\delta$ .

## 2 The eightfold degeneracy

In Ref. [16] it has been noticed that the appearance probability  $P_{\alpha\beta}$  obtained for neutrinos at a fixed energy and baseline with input parameter  $(\bar{\theta}_{13}, \bar{\delta})$  has no unique solution. Indeed, the equation

$$P_{\alpha\beta}(\bar{\theta}_{13}, \bar{\delta}) = P_{\alpha\beta}(\theta_{13}, \delta) \quad (1)$$

has a continuous number of solutions. The locus of the  $(\theta_{13}, \delta)$  plane satisfying this equation is called “equiprobability curve”. Considering the equiprobability curves for neutrinos and antineutrinos with the same energy (and the same input parameters), the following system of equations ( $\pm$  referring to neutrinos and antineutrinos respectively)

$$P_{\alpha\beta}^\pm(\bar{\theta}_{13}, \bar{\delta}) = P_{\alpha\beta}^\pm(\theta_{13}, \delta) \quad (2)$$

has two intersections: the input pair  $(\bar{\theta}_{13}, \bar{\delta})$  and a second, energy dependent, point. This second intersection introduces an ambiguity in the measurement of the physical values of  $\theta_{13}$  and  $\delta$ : the so-called *intrinsic clone* solution. Knowing the two probabilities of Eq. (2) is consequently not enough for solving the intrinsic degeneracy. One needs to add more information.

Unfortunately the appearance of the intrinsic degeneracy is only a part of the “clone problem”. As it was made clear in [17, 18, 19], two other sources of ambiguities arise due to the present (and near future) ignorance of the sign of the atmospheric mass difference,  $s_{atm} = \text{sign}[\Delta m_{23}^2]$  and the  $\theta_{23}$  octant, namely  $s_{oct} = \text{sign}[\tan(2\theta_{23})]$ . These two discrete variables assume the values  $\pm 1$ , depending on the physical assignments of the  $\Delta m_{23}^2$  sign ( $s_{atm} = 1$  for  $m_3^2 > m_2^2$  and  $s_{atm} = -1$  for  $m_3^2 < m_2^2$ ) and of the  $\theta_{23}$ -octant ( $s_{oct} = 1$  for  $\theta_{23} < \pi/4$  and  $s_{oct} = -1$  for  $\theta_{23} > \pi/4$ ). As a consequence, future experiments will have as ultimate goal the measure of the two continuous variables  $\theta_{13}$  and  $\delta$  plus the two discrete variables  $s_{atm}$  and  $s_{oct}$ .

Moreover it should be noticed that experimental results are not given in terms of oscillation probabilities but of number of charged leptons observed in a specific detector. It has been noticed [20] that clones location calculated starting from the probability or the number of events can be significantly different. We must therefore integrate the oscillation probability over the neutrino flux, the  $\nu N$  cross-section and the detector efficiency  $\epsilon(E_\mu)$ . From these considerations it follows that Eq. (2) should be more correctly replaced by:

$$N_{\bar{\beta}}^{\pm}(\bar{\theta}_{13}, \bar{\delta}; \bar{s}_{atm}, \bar{s}_{oct}) = N_{\beta}^{\pm}(\theta_{13}, \delta; s_{atm} = \bar{s}_{atm}; s_{oct} = \bar{s}_{oct}). \quad (3)$$

In Eq. (3) we have implicitly assumed to know the right sign and the right octant for the atmospheric mass difference and angle. As these quantities are unknown (and presumably they will still be unknown at the time of the neutrino facilities considered in this paper) the following systems of equations should be considered as well:

$$N_{\bar{\beta}}^{\pm}(\bar{\theta}_{13}, \bar{\delta}; \bar{s}_{atm}, \bar{s}_{oct}) = N_{\beta}^{\pm}(\theta_{13}, \delta; s_{atm} = -\bar{s}_{atm}, s_{oct} = \bar{s}_{oct}) \quad (4)$$

$$N_{\bar{\beta}}^{\pm}(\bar{\theta}_{13}, \bar{\delta}; \bar{s}_{atm}, \bar{s}_{oct}) = N_{\beta}^{\pm}(\theta_{13}, \delta; s_{atm} = \bar{s}_{atm}, s_{oct} = -\bar{s}_{oct}) \quad (5)$$

$$N_{\bar{\beta}}^{\pm}(\bar{\theta}_{13}, \bar{\delta}; \bar{s}_{atm}, \bar{s}_{oct}) = N_{\beta}^{\pm}(\theta_{13}, \delta; s_{atm} = -\bar{s}_{atm}, s_{oct} = -\bar{s}_{oct}) \quad (6)$$

Solving the four systems of Eqs. (3)-(6) will result in obtaining the true solution plus additional *clones* to form an eightfold degeneracy [19]. These eight solutions are respectively:

- the true solution and its *intrinsic clone*, obtained solving the system in Eq. (3);
- the  $\Delta m_{23}^2$ -sign clones (hereafter called *sign clones*) of the true and intrinsic solution, obtained solving the system in Eq. (4);
- the  $\theta_{23}$ -octant clones (hereafter called *octant clones*) of the true and intrinsic solution, obtained solving the system in Eq. (5);
- the  $\Delta m_{atm}^2$ -sign  $\theta_{23}$ -octant clones (hereafter called *mixed clones*) of the true and intrinsic solution, obtained solving the system in Eq. (6).

A complete description of the clone location has been done in [20] and we refer to that article for all the theoretical details. In this paper we are interested in presenting a detailed analysis of a concrete experimental facility, that we are going to describe in the following Sections.

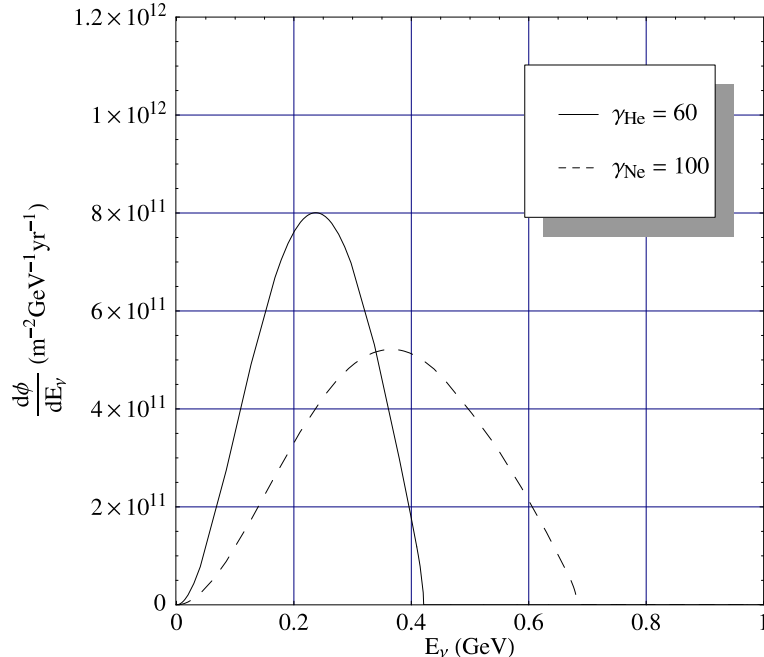


Figure 1:  $\beta$ -Beam fluxes at the Fréjus location (130 km baseline) as a function of the neutrino energy for the two specific  $\gamma$  values shown in the legend.

### 3 Neutrino beam facilities at CERN

In this Section we summarize some of the technical details of the two considered neutrino beams, the standard  $\beta$ -Beam (Section 3.1) and the Super-Beam (Section 3.2). Both beams are directed from CERN toward the underground Fréjus laboratory, where it has been proposed to locate a 1 Megaton UNO-like [21] water Cerenkov detector with a 440 Kt fiducial mass. The considered baseline is thus  $L = 130$  Km for both beams. Therefore, in order to be at the maximum of the atmospheric neutrino oscillations, the peaks of the energy spectra have been chosen of order few hundred MeV.

#### 3.1 The $\beta$ -Beam

The  $\beta$ -Beam concept was first introduced in Ref. [22]. It involves producing a beam of  $\beta$ -unstable heavy ions, accelerating them to some reference energy, and allowing them to decay in the straight section of a storage ring, resulting in a very intense neutrino beam. Two ions have been identified as ideal candidates:  ${}^6\text{He}$ , to produce a pure  $\bar{\nu}_e$  beam, and  ${}^{18}\text{Ne}$ , to produce a  $\nu_e$  beam. The “golden” [23] sub-leading transitions  $\nu_e \rightarrow \nu_\mu$  and  $\bar{\nu}_e \rightarrow \bar{\nu}_\mu$  can be measured through the appearance of muons in a distant detector.

The neutrino beam energy depends on the  $\gamma$  of the parent ions in the decay ring. For the scenario considered in this paper the  $\gamma$  ratio for the two ions has been fixed to

Element	End-Point (MeV)	Decay Fraction
$^{18}\text{Ne}$	34.114	92.1%
	23.699	7.7%
	17.106	0.2%
$^6\text{He}$	35.078	100%

Table 1:  $^{18}\text{Ne}$  and  $^6\text{He}$   $\beta$ -decay channels and relative end-point energies from [24].

be  $\gamma(^6\text{He})/\gamma(^{18}\text{Ne}) = 3/5$  [13]. This constraint comes from the request to accelerate in the same accelerator at the same time ions with different atomic mass. The optimal  $\gamma$  values that match the CERN-Fréjus distance have been found to be  $\gamma(^6\text{He}) = 60$  and  $\gamma(^{18}\text{Ne}) = 100$ . The mean neutrino energies of the  $\bar{\nu}_e, \nu_e$  beams corresponding to this configuration are 0.23 GeV and 0.37 GeV, respectively. On the other hand the energy resolution is very poor at these energies, given the influence of Fermi motion and other nuclear effects. Therefore, in the following all the sensitivities are computed for a counting experiment with no energy cuts.

A flux of  $2.9 \times 10^{18}$   $^6\text{He}$  decays/year and  $1.1 \times 10^{18}$   $^{18}\text{Ne}$  decays/year, as discussed in Ref. [13], will be assumed. Fig. 1 shows the  $\beta$ -Beam neutrino fluxes computed at the 130 Km baseline, keeping  $m_e \neq 0$ , following the formulas derived in Ref. [11], while in Ref. [13] the fluxes are calculated in the  $m_e = 0$  approximation. Be aware of the fact that even if  $m_e$  effects seem negligible, their inclusion could be sizable due to the dramatic cross-section suppression of low energy neutrinos<sup>2</sup>. Furthermore, in our calculations we take into account the fact that the  $^{18}\text{Ne}$  has three different decay modes, each with a different end-point energy, see Table 1.

### 3.2 The Super-Beam

The Super-Beam is a conventional neutrino beam, but with a higher proton intensity. Therefore, it has the advantages of a high intensity flux and of a well proved technology. On the other hand its composition ( $\nu_\mu$  main component, if  $\pi^+$  are focused, plus a small admixture of  $\bar{\nu}_\mu, \nu_e$  and  $\bar{\nu}_e$ ) is affected by large systematic uncertainties that limit the sensitivity in searching for neutrino oscillations mainly  $\nu_\mu \rightarrow \nu_e$ .

As baseline for this work we consider a Super-Beam based on a 2.2 GeV proton beam of 4 MW power SPL, described in Ref. [14]. The predicted energy spectra and fluxes for the main components have been computed starting from a full simulation of the neutrino beamline [25], assuming a decay tunnel length of 60 m. The neutrino fluxes expected at the Fréjus location are shown in Fig. 2. The average energy of the

---

<sup>2</sup>For example we checked that by using the cross-sections discussed in Section 4, the rate, for both neutrinos and antineutrinos, computed in the  $m_e = 0$  approximation is about 20% smaller than in the case  $m_e \neq 0$ .

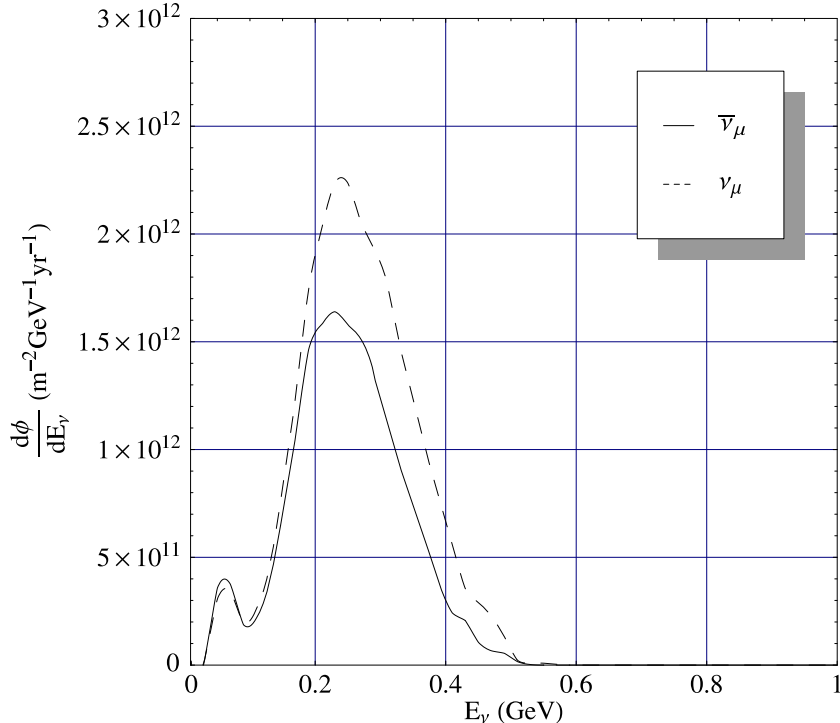


Figure 2: *SPL Super-Beam fluxes at the Fréjus location (130 km baseline) as a function of the neutrino energy [25].*

neutrino and antineutrino beams is 0.27 GeV and 0.25 GeV, respectively.

## 4 Neutrino cross-sections

The present knowledge of the neutrino and antineutrino cross-sections for energies below 1 GeV is very poor [26]: either there are very few data, as for neutrinos, or there are no data available at all, as for antineutrinos. On top of that, the few available data have not been taken on water, the target we are interested in, and the extrapolation from different nuclei is complicated by nuclear effects that at the considered energies play an important role. For this calculation we adopted the cross-sections on water shown in Fig. 3 [29]. Notice the difference between the  $\nu_e N$  and  $\bar{\nu}_e N$  cross-sections: the former, being an interaction between the  $\nu_e$  and a neutron inside the oxygen nucleus, is affected by nuclear effects and thus shows a threshold energy. The latter is mainly a  $\bar{\nu}_e$  interaction with the protons of the two hydrogens, approximately free. This effect, although less pronounced, is visible also for  $\nu_\mu$  and for  $\bar{\nu}_\mu$ . This feature is quite relevant for neutrino/antineutrino of hundreds of MeV energy, region where different cross-sections can easily differ by a factor 2. Compare for example our Fig. 3 with Fig. 3 of Ref. [11] where NUANCE cross-sections [27] are plotted. These differences can explain the (sometimes relevant) discrepancies within the numbers of charged-

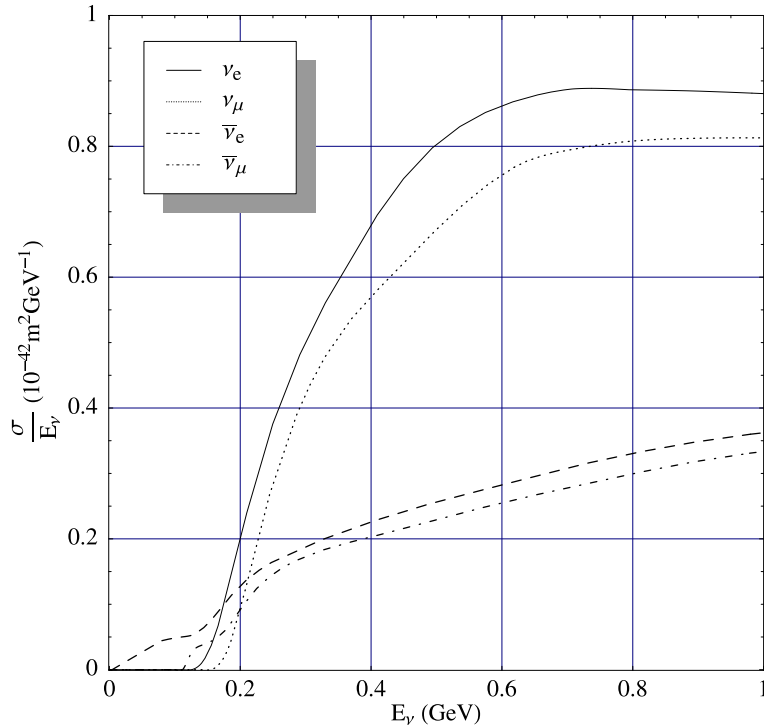


Figure 3: *Cross-sections on water as a function of the neutrino energy [29].*

current interactions and oscillated events predicted in different analyzes. Be aware that there are other nuclear effects (see [28] and references therein) not included yet in any of the available calculations that could play an important effect at the cross-section threshold energy.

With our calculations the expected number of charged-current events with a  $\beta$ -Beam without oscillations per kton-year is 30.3 and 4.4 for  $\nu_e$  and  $\bar{\nu}_e$ , respectively. While in Ref. [11], they quote 32.8 and 4.7 for  $\nu_e$  and  $\bar{\nu}_e$ , respectively. We verify, that using the NUANCE cross-sections we are able to reproduce exactly their results as well as those of Ref. [13]. As far as the Super-Beam is concerned, the expected number of charged-current events with a Super-Beam without oscillations per kton-year is 27.6 and 7.2 for  $\nu_\mu$  and  $\bar{\nu}_\mu$ , respectively. We verify, that using the NUANCE cross-sections we are able to reproduce within 5% the results of Ref. [30], while we still found a discrepancy of more than 30% with those quoted in Ref. [13].

Besides the absolute value of the cross-sections, another important unknown is their shape. Indeed, as it will be discussed later, some of the backgrounds have a neutrino energy threshold. Therefore, the expected background strongly depends on the adopted model.

At the time the neutrino complex would become operational the cross-sections will be measured precisely. However, nowadays we have the problem to compute the physics potential of a facility having in mind that the expected number of signal and



background events strongly depend on the adopted calculation.

A facility where the neutrino fluxes are known with great precision is the ideal place where to measure neutrino cross-sections. At a  $\beta$ -Beam the neutrino fluxes are completely defined by the parent ions  $\beta$ -decay properties and by the number of ions in the decay ring. A close detector of  $\sim 1$  Kton placed at a distance of about 1 Km from the decay ring could then measure the relevant neutrino cross-sections. Furthermore the  $\gamma$  factor of the accelerated ions can be varied. In particular a scan can be initiated below the background production threshold, allowing a precise measurement of the cross-sections for resonant processes.

Unfortunately, there are no studies available on the ultimate precision achievable at future facilities in measuring the charged-current cross-sections. A first attempt to estimate the ultimate systematic error achievable in the cross-section measurements at future facilities was given in [9]. By assuming the  $\beta$ -Beam complex described before a systematic error of 2% was estimated.

## 5 $\theta_{13}$ and $\delta$ sensitivity

In this Section we present our results for the sensitivity to  $\theta_{13}$  and  $\delta$  at the CERN-based standard  $\beta$ -Beam and SPL Super-Beam. The sensitivity to the  $\theta_{13}$  and  $\delta$  parameters has been evaluated using the following reference values for the solar and atmospheric parameters:  $\Delta m_{12}^2 = 7.3 \times 10^{-5} \text{eV}^2$ ,  $\theta_{12} = 35^\circ$ ,  $\Delta m_{23}^2 = 2.5 \times 10^{-3} \text{eV}^2$  and  $\theta_{23} = 40^\circ$ .

We proceed first summarizing the backgrounds for both the facilities (Sections 5.1-5.2) and then studying the  $\beta$ -Beam and the Super-Beam separately and in combination (Section 5.3).

### 5.1 Signal and background at a standard $\beta$ -Beam

The signal in a  $\beta$ -Beam looking for  $\nu_e \rightarrow \nu_\mu$  ( $\bar{\nu}_e \rightarrow \bar{\nu}_\mu$ ) oscillations would be the appearance of  $\nu_\mu(\bar{\nu}_\mu)$  charged-current events, mainly via quasi-elastic interactions, in a pure  $\nu_e(\bar{\nu}_e)$  beam. Background rates and signal efficiencies have been studied, by means of a full simulation based on the NUANCE code [27], in Refs. [11, 13]. In this paper, we make use of those results for the beam and detector fractional background and compute the expected number of oscillated events by using the fluxes of Fig. 1, the cross-section on water of Fig. 3, the full three-families oscillation probability in matter and the  $\nu_\mu$  detection efficiency of Fig. 4.

Given its excellent purity (neither  $\nu_\mu$  nor  $\bar{\nu}_\mu$  are in the initial beam) the background in a detector exploiting a  $\beta$ -Beam can be generated either by inefficiencies in particle identification, such as mis-identification of pions produced in neutral-current single-pion resonant interactions, electrons (positrons) mis-identified as muons, or by external sources such as atmospheric neutrino interactions.

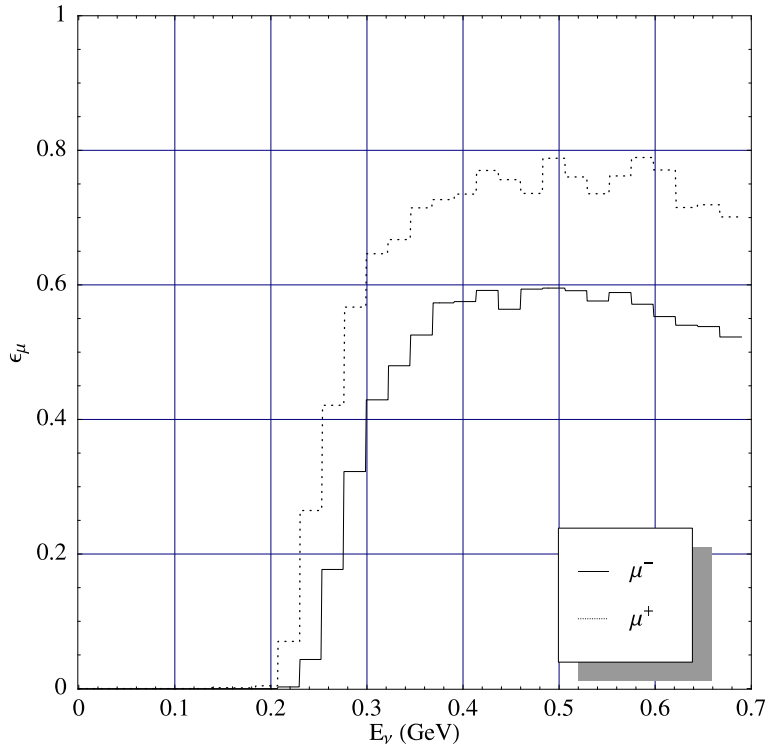


Figure 4: *Reconstruction efficiency as a function of the true neutrino energies for  ${}^6\text{He}$  ( $\bar{\nu}_e$ ) and  ${}^{18}\text{Ne}$  ( $\nu_e$ ) in water [11].*

The pion background has a threshold at neutrino energies of about 0.45 GeV, and is highly suppressed at the  $\beta$ -Beam energies. The electron background is almost completely suppressed by the request of the detection of a delayed Michel electron following the muon track. If a bunch length of 10 ns (which seems feasible) is assumed, this background becomes negligible [13]. Moreover, out-of-spill neutrino interactions can be used to normalize this background to the 1% accuracy level.

The event rates for a 4400 kt-y exposure are also given in Table 2, both for non-oscillated and oscillated  $\nu_e, \bar{\nu}_e$ , with  $\nu_e \rightarrow \nu_\mu$  oscillation probability computed for  $\theta_{13} = 10^\circ$  and  $\delta = 90^\circ$ , and  $\theta_{13} = 1^\circ$  and  $\delta = -90^\circ, 90^\circ$ . In Table 2 the expected beam and detector backgrounds (derived from the fractional background in Refs. [11, 13]) are also given.

Finally, some comments on the overall systematic error and on the expected background are in order. The ultimate precision on cross-sections achievable at future facilities is about 2%. This value has been also assumed in Ref. [13] as an overall systematic error. However, it does not take into account possible systematic errors on the detection efficiencies and on the neutrino fluxes. In order to be conservative, we adopted an overall systematic error of 5%. Nonetheless, we also studied the impact on the physics potential going from 5% to 2%.

$\theta_{13}$	$\delta$	$s_{atm}$	$N_\nu$	$N_{\bar{\nu}}$	$P_{\nu_e\nu_\mu}(E = 0.37)$	$P_{\bar{\nu}_e\bar{\nu}_\mu}(E = 0.23)$
No Osc.			133205	19557		
10°	0°	+	2472	457	$5.48 \times 10^{-2}$	$5.17 \times 10^{-2}$
10°	0°	-	1918	445	$4.35 \times 10^{-2}$	$6.57 \times 10^{-2}$
1°	90°	+	75	1	$1.85 \times 10^{-3}$	$1.71 \times 10^{-4}$
1°	90°	-	73	1	$1.79 \times 10^{-3}$	$1.44 \times 10^{-4}$
1°	-90°	+	8	18	$9.99 \times 10^{-5}$	$3.35 \times 10^{-3}$
1°	-90°	-	8	20	$9.63 \times 10^{-5}$	$3.50 \times 10^{-3}$
Beam back.			0	0		
Detector back.			360	1		

Table 2: *Event rates for a 10 years exposure at a standard  $\beta$ -Beam. The oscillated charged-current events for different values of  $\theta_{13}, \delta$  and sign of the atmospheric mass difference,  $s_{atm}$ , for both neutrinos and antineutrinos are given. For comparison with literature we show here the values obtained with the reference parameters but  $\theta_{23} = 45^\circ$ . The oscillation probabilities at the mean neutrino/antineutrino energy (in GeV) are also shown.*

As far as the background is concerned, we would like to stress that it is due to the coherent pion production process, with a threshold at 0.45 GeV. Therefore, following the arguments of Section 4, it strongly depends on the adopted model. We checked that our results are stable against variations of the background in the neutrino channel, while this is not the case for the antineutrino channel. In absence of a full Monte Carlo simulation, in the following calculations we adopt the central values given in Tab. 2. The impact of an increase of this background on the sensitivity is discussed in Section 5.4.

## 5.2 Signal and background at the Super-Beam

The search for  $\nu_\mu \rightarrow \nu_e$  ( $\bar{\nu}_\mu \rightarrow \bar{\nu}_e$ ) appearance with a Super-Beam is complicated by the  $\nu_e(\bar{\nu}_e)$  contamination of the beam. Indeed, contrary to the case of the  $\beta$ -Beam where the beam-induced background is absent (see Table 2), for the Super-Beam a significant background from  $\nu_e(\bar{\nu}_e)$  charged-current interactions must be considered, resulting in a loss of sensitivity. In a water Cerenkov detector the appearance of a  $\nu_e(\bar{\nu}_e)$  signal is detected by exploiting the high efficiency and purity of the detector in identifying electrons and muons in low multiplicity interactions.

Besides the  $\nu_e(\bar{\nu}_e)$  contamination of the beam, the main sources of background are the charged-current interactions of  $\nu_\mu(\bar{\nu}_\mu)$  and the production of  $\pi^0$  in neutral-current interactions. The total background has been computed following the fractional backgrounds given in Ref. [14].

To compute the expected number of non-oscillated and oscillated events we have used the fluxes of Fig. 2, the cross-section on water of Fig. 3, the full three-families oscillation probability in matter and the electron detection efficiency computed in Ref. [14]: 70.7% and 67.1% for  $\nu_\mu \rightarrow \nu_e$  and  $\bar{\nu}_\mu \rightarrow \bar{\nu}_e$ , respectively. The corresponding beam and detector background has been computed making use of the results quoted in Ref. [13, 14].

As far as the signal and background systematic errors, we followed the arguments given in Ref. [31], but we have considered only 2% and 5%, and finally presented results for the worst case. The two cases are on the other hand considered when sensitivity plots are presented.

The event rates are given in Table 3. Note that, given the difference in cross-section between neutrino and antineutrino and that it is not possible to run a Super-Beam with both polarities at the same time, to get comparable statistics the run should be asymmetric in time: in Ref. [13], 2 years run with main component  $\nu_\mu$  and 8 years run with main component  $\bar{\nu}_\mu$  were assumed. It is however not clear that having a comparable statistics is really necessary to get a good  $\theta_{13}, \delta$  signal. In the case of the Neutrino Factory, for example, it has been shown that a combination of two different detectors, the first looking for  $\nu_e \rightarrow \nu_\mu$  oscillations with high statistics and the second for  $\nu_e \rightarrow \nu_\tau$  with low statistics is extremely useful to solve some of the parameter space degeneration [32]. Indeed, with a 2+8 run the gain in the  $\bar{\nu}_\mu$  flux is compensated by a loss in the  $\nu_\mu$  flux. We have therefore also run in a symmetric 5+5 years configuration: our results indicate that the two choices work similarly on the average, with one or the other performing slightly better depending on the particular region of the  $(\theta_{13}, \delta)$  parameter space. In the rest of the paper, to establish direct comparison with [13], we adopt the 2+8 configuration.

### 5.3 Extraction of neutrino oscillation parameters in presence of signal

The sensitivity to the  $\theta_{13}$  and  $\delta$  parameters has been evaluated by assuming the signal and background rates reported in the previous Sections and the following input values:  $\Delta m_{12}^2 = 7.3 \times 10^{-5} \text{eV}^2$ ,  $\theta_{12} = 35^\circ$ ,  $\Delta m_{23}^2 = 2.5 \times 10^{-3} \text{eV}^2$ , and  $\theta_{23} = 40^\circ$ . Since the sign of  $\Delta m_{23}^2$  and the  $\theta_{23}$ -octant are unknown, fits to both  $\text{sign}[\Delta m_{23}^2] = \pm 1$  and  $\text{sign}[\tan(2\theta_{23})] = \pm 1$  have been performed. In the particular case  $\theta_{23} = 45^\circ$ , four out of eight solutions of the systems of Eqs. (3)-(6) disappear and only fits to the wrong assignment of  $\text{sign}(\Delta m_{23}^2)$  must be performed. However, since at a given confidence level the contours for the allowed regions (around the theoretical location of the true solution, the intrinsic clone and of the two sign clones) are not qualitatively different from those we get for  $\theta_{23} = 40^\circ$ , we have opted to present results for this last case, only.

Our results for two specific values,  $\bar{\theta}_{13} = 1^\circ, 7^\circ$ , are presented in Figs. 5-7. In each

$\theta_{13}$	$\delta$	$s_{atm}$	$N_\nu$	$N_{\bar{\nu}}$	$P_{\nu_\mu\nu_e}(E = 0.27)$	$P_{\bar{\nu}_\mu\bar{\nu}_e}(E = 0.25)$
No Osc.			24245	25467		
10	0	+	1200	1013	$6.44 \times 10^{-2}$	$5.68 \times 10^{-2}$
10	0	-	1033	1089	$5.78 \times 10^{-2}$	$6.52 \times 10^{-2}$
1	90	+	2	52	$2.11 \times 10^{-5}$	$3.13 \times 10^{-3}$
1	90	-	3	54	$3.20 \times 10^{-5}$	$3.27 \times 10^{-3}$
1	-90	+	50	5	$3.01 \times 10^{-3}$	$6.96 \times 10^{-5}$
1	-90	-	49	5	$2.89 \times 10^{-3}$	$5.16 \times 10^{-5}$
Beam back.			92	110		
Detector back.			24	56		

Table 3: *Event rates for an exposure at a standard Super-Beam. The oscillated charged-current events for different values of  $\theta_{13}$ ,  $\delta$  and sign of the atmospheric mass difference,  $s_{atm}$  for both neutrinos (2 years data taking) and antineutrinos (8 years of data taking) are given. For comparison with literature we show here the values obtained with the reference parameters but  $\theta_{23} = 45^\circ$ . The oscillation probabilities at the mean neutrino/antineutrino energy (in GeV) are also shown.*

figure we plot the 90 % CL contours for the two considered values of  $\bar{\theta}_{13}$  and a fixed value of  $\delta$ :  $\bar{\delta} = 90^\circ$  (Fig. 5),  $\bar{\delta} = 0$  (Fig. 6) and  $\bar{\delta} = -90^\circ$  (Fig. 7). From top to bottom, the results for the  $\beta$ -Beam, for the Super-Beam and for the combination of the two are presented.

In every separate case, the four possible choices of the discrete variables  $s_{atm}, s_{oct}$  are reported: continuous lines stand for the true solution and the intrinsic degeneracy (right sign( $\Delta m_{23}^2$ ) and right  $\theta_{23}$ -octant); dashed lines stand for the sign degeneracy (wrong sign( $\Delta m_{23}^2$ ) and right  $\theta_{23}$ -octant); dot-dashed lines stand for the octant degeneracy (right sign( $\Delta m_{23}^2$ ) and wrong  $\theta_{23}$ -octant); dotted lines stand for the mixed degeneracy (wrong sign( $\Delta m_{23}^2$ ) and wrong  $\theta_{23}$ -octant). In all the figures, the light (red) circle shows the input value. The dark (black) circles in the plots for the  $\beta$ -Beam and the Super-Beam represent the theoretical clone locations computed as in Ref. [20] for the two facilities considered in this paper. They have been included to show the rather good agreement between the theoretical computation and the output of the fits. Notice that for  $\bar{\theta}_{13} = 7^\circ$  some of the theoretical clones are missing. Indeed, an analytic solution of the systems in Eqs. (3)-(6) is not always found for large  $\bar{\theta}_{13}$  values, see [20] for details.

Notice first that the impact of the octant-ambiguity in all the considered cases is by far more relevant for large values of  $\bar{\theta}_{13}$  than for small values. For the three values of  $\delta$  that we have analyzed we get the octant clones with a  $\Delta\theta_{13} \sim 1^\circ$  shift with respect to the true solution when  $\bar{\theta}_{13} = 7^\circ$ , whereas we get a significantly smaller shift when  $\bar{\theta}_{13} = 1^\circ$ . This comment apply both to the  $\beta$ -Beam and the Super-Beam results: indeed, when the octant-ambiguity is considered, both facilities show pretty similar

contours. This is why, as a general result, the combination of the two facilities does not solve this ambiguity. Even in the case of  $\bar{\theta}_{13} = 7^\circ$ , for which a significant statistics is accumulated for both facilities, the bottom plot of Figs. 5-7 shows that at 90 % CL the true solution and the octant ambiguity survive for the three values of  $\delta$  considered.

Concerning the sign ambiguity we notice that, for both facilities and for both considered values of  $\bar{\theta}_{13} = 1^\circ, 7^\circ$ , the allowed regions corresponding to the clone solutions overlap with the true solution in a significant way. As a consequence the combination of the two facilities, albeit reducing the 90 % CL contours, does not solve the sign ambiguity, either. However, contrary to the case of the octant degeneracy treated above, this does not affect the measurement of the two continuous unknowns  $\theta_{13}$  and  $\delta$ . For large  $\bar{\theta}_{13}$ , a considerably good measurement of both quantities is achieved, with no clue on the mass hierarchy. An exception to this statement is the particular case  $\bar{\theta}_{13} = 7^\circ, \bar{\delta} = 0$ , for which the sign clones are quite definite regions located in different places for the  $\beta$ -Beam and the Super-Beam. This actually allows the cancellation of some of the allowed regions when combining the two facilities. The ambiguities are however not solved, since clone regions survive near  $\delta = 180^\circ$ .

Discussing the mixed ambiguity, we notice that much of what was said for the sign degeneracies can be repeated in this case: the only difference being that allowed regions around mixed clones overlap significantly with the octant degeneracy, and not with the true solution as it was the case for the sign degeneracy. As a consequence, mixed clones survive after the combination of the two facilities. This comment applies to all the considered input pairs, with the exception of the  $\bar{\theta}_{13} = 7^\circ, \bar{\delta} = 0$  case (as for the sign ambiguity) and of  $\bar{\theta}_{13} = 7^\circ, \bar{\delta} = -90^\circ$ , for which no mixed ambiguity is present in the Super-Beam.

We observe that in general four allowed regions are still present after adding data from the  $\beta$ -Beam and the Super-Beam at large  $\bar{\theta}_{13}$  (with the exception  $\bar{\theta}_{13} = 7^\circ, \bar{\delta} = -90^\circ$ , for which the mixed clone is absent after combination). These four regions either overlap in pairs (case of  $\bar{\delta} = 90^\circ, -90^\circ$ ) or stay well apart (case of  $\bar{\delta} = 0$ ), in all cases allowing a measure of the two continuous parameters but not of the two discrete parameters. On the other hand, for small  $\bar{\theta}_{13}$  we are clearly on the sensitivity limit of these experiments: no clear measure of  $\delta$  is possible (at 90 % CL we can just state if  $\delta$  is positive or negative) and no discrete ambiguity is solved.

From the results reported in the top plots of Figs. 5-7, it is clear that by using the  $\beta$ -Beam or the Super-Beam as isolated experiment it is not possible to solve any of the degeneracies, although for large enough  $\bar{\theta}_{13}$  a first estimate of the two continuous parameters  $\theta_{13}$  and  $\delta$  can be attempted. Even when combining the two experiments we have found that as a general result the discrete parameters are not measured. These results are in contrast with the statement of [13] “*We stress the fact that an experiment working at very short baselines has the smallest possible parameter degeneracies and ambiguities and it is the cleanest possible environment where to look for genuine leptonic CP violation effects*”. The correct statement is that in many cases the discrete

ambiguities, although not solved, does not affect in a significant way the measure of the continuous parameters. Notice, however, that in general multiple solutions are found with either larger uncertainties in both parameters when these regions overlap or a proliferation of disconnected regions in the parameter space<sup>3</sup>.

## 5.4 Exclusion plots in absence of signal

In Figs. 8, 9, 10 we present exclusion plots in the absence of a signal for the  $\beta$ -Beam, the SPL-Super-Beam and their combination. The different lines represent, with the notation used in the previous figures, different choices of the two discrete parameters  $s_{atm}, s_{oct}$ .

In the upper plot of Fig. 8, 9, 10 we draw the 90% CL contour defining the sensitivity limit on  $\theta_{13}$  in case of absence of a signal, with  $\delta$  as a free parameter. Notice how the sensitivity limit spans a region from  $\sim 0.5^\circ$  to  $2.5^\circ$ , the less stringent limit being for  $\delta = 0$ . A significant loss in sensitivity for this value of  $\delta$  is induced by the unsolved discrete ambiguities, whereas for other  $\delta$  values the worse limit is generally given by the true solution. It is worth noting that the  $\beta$ -Beam plots of Fig. 8 show a better sensitivity for  $\delta = 90^\circ$  than for  $\delta = -90^\circ$  (see also [13]). This result reflects the expected large signal statistics for neutrinos at  $\delta = 90^\circ$  and the small background (1 event) for antineutrinos. Being the background affected by large uncertainties (see Section 4), we checked that, if the expected number of background events increases, the sensitivity enhancement disappears and the plots become symmetric in  $\delta$ . In the case of the Super-Beam, Fig. 9, we notice no asymmetry in  $\delta$  in both plots. This is a consequence of the more symmetric background reported in Tab. 3 for both the neutrino and antineutrino beams. Furthermore, we point out that the effect of the degeneracies on the sensitivity is much lower than in the case of the  $\beta$ -Beam: in both plots it can be seen how the different excluded regions coming from different choices of the discrete parameters  $s_{atm}$  and  $s_{oct}$  overlap significantly.

In the lower plot of Figs. 8, 9, 10 we draw the 90% CL contour in the absence of a CP violating signal (that can be interpreted as  $\delta = 0^\circ$ ) for fixed values of  $\theta_{13}$ . In this case it is clearly visible how the true solution define an upper bound on  $|\delta| \leq 30^\circ - 40^\circ$ , whereas the sign degeneracy draw a lower bound for  $|\pi - \delta| \geq 150^\circ - 170^\circ$ . The octant and mixed degeneracy, on the other hand, do not play a significant role in this sensitivity plot apart for excluding small regions of parameter space around  $\theta_{13} \simeq 4^\circ$  and positive  $\delta$ .

We also studied the dependence of the sensitivity on the systematic error for the combined  $\beta$ -Beam and Super-Beam setup. The results are shown in Fig. 10, from which it can be noticed that there is not a strong impact on the sensitivity going from 5% to 2%.

---

<sup>3</sup>The presence and the locations of the clones as derived in this paper are in rather good agreement with the analytical calculations quoted in [20].

## 6 Conclusion

Over the past years the possibility to build a CERN neutrino complex, based on the novel concept of the  $\beta$ -Beam and on a neutrino Super-Beam, that exploits a 1 Mega-ton water Cerenkov detector located at the Fréjus underground laboratory (130 km baseline) has been put forward. In this paper we study for the first time the eightfold degeneracy for such a scenario.

After a brief theoretical discussion about the eightfold degeneracy and a short description of the  $\beta$ -Beam and Super-Beam facilities, we focus on the neutrino and antineutrino cross-sections at low energies. At the time the neutrino complex will become operational, it would be possible to measure with high accuracy the cross-sections. However, nowadays we have the problem to compute the physics potential of a facility having in mind that the expected number of signal and background events strongly depend on the adopted calculation. In particular we pointed out that the background in the antineutrino channel of a  $\beta$ -Beam depends on the shape and absolute value of the cross-section and that this background can significantly affect the sensitivity to  $\theta_{13}$  and  $\delta$ .

From the results reported in this paper it is clear that by using the  $\beta$ -Beam or the Super-Beam alone it is not possible to solve all the degeneracies, although for large enough  $\bar{\theta}_{13}$  a first estimate of the two continuous parameters  $\theta_{13}$  and  $\delta$  can be attempted. Even when combining the two experiments we have found that as a general result the discrete parameters are not measured. In many cases the discrete ambiguities, although not solved, do not affect in a significant way the measurement of the continuous parameters. Notice, however, that in general multiple solutions are found with either larger uncertainties in both parameters when these regions overlap or a proliferation of disconnected regions in the parameter space.

As a final comment we want to stress that being the experiment discussed in this paper a “counting experiment”, the small differences between the fluxes are averaged-out. Therefore, being  $N_{evts}(\nu_\mu \rightarrow \nu_e) \simeq T(N_{evts}(\nu_e \rightarrow \nu_\mu))$ , the combination (synergy) of a  $\beta$ -Beam and of a Super-Beam only determines an increase of statistics for both neutrinos and antineutrinos. Therefore, there is not a real synergy.

## Acknowledgments

We would like to thank B. Gavela, S. Gilardoni, J. Gomez-Cadenas, P. Hernandez, P. Lipari, O. Mena, M. Mezzetto and F. Terranova for useful discussions during the preparation of this paper.



## References

- [1] Y. Fukuda *et al.* [Super-Kamiokande Collaboration], Phys. Rev. Lett. **81** (1998) 1562 [arXiv:hep-ex/9807003];  
M. Ambrosio *et al.* [MACRO Collaboration], Phys. Lett. B **517** (2001) 59 [arXiv:hep-ex/0106049].
- [2] M. H. Ahn *et al.* [K2K Collaboration], Phys. Rev. Lett. **90** (2003) 041801 [arXiv:hep-ex/0212007].
- [3] B. T. Cleveland *et al.*, Astrophys. J. **496** (1998) 505;  
J. N. Abdurashitov *et al.* [SAGE Collaboration], Phys. Rev. C **60** (1999) 055801 [arXiv:astro-ph/9907113];  
W. Hampel *et al.* [GALLEX Collaboration], Phys. Lett. B **447** (1999) 127;  
S. Fukuda *et al.* [Super-Kamiokande Collaboration], Phys. Rev. Lett. **86** (2001) 5651 [arXiv:hep-ex/0103032];  
Q. R. Ahmad *et al.* [SNO Collaboration], Phys. Rev. Lett. **87** (2001) 071301 [arXiv:nucl-ex/0106015].
- [4] K. Eguchi *et al.* [KamLAND Collaboration], Phys. Rev. Lett. **90** (2003) 021802 [arXiv:hep-ex/0212021].
- [5] C. Athanassopoulos *et al.* [LSND Collaboration], Phys. Rev. Lett. **81** (1998) 1774 [arXiv:nucl-ex/9709006];  
A. Aguilar *et al.* [LSND Collaboration], Phys. Rev. D **64** (2001) 112007 [arXiv:hep-ex/0104049].
- [6] I. Stancu *et al.* [MiniBooNE collaboration], FERMILAB-TM-2207.
- [7] B. Pontecorvo, Sov. Phys. JETP **6** (1957) 429 [Zh. Eksp. Teor. Fiz. **33** (1957) 549];  
Z. Maki, M. Nakagawa and S. Sakata, Prog. Theor. Phys. **28** (1962) 870;  
B. Pontecorvo, Sov. Phys. JETP **26** (1968) 984 [Zh. Eksp. Teor. Fiz. **53** (1967) 1717];  
V. N. Gribov and B. Pontecorvo, Phys. Lett. B **28** (1969) 493.
- [8] M. Apollonio *et al.* [CHOOZ Collaboration], Phys. Lett. B **466** (1999) 415 [arXiv:hep-ex/9907037];  
M. Apollonio *et al.* [CHOOZ Collaboration], Eur. Phys. J. C **27** (2003) 331 [arXiv:hep-ex/0301017].
- [9] M. Apollonio *et al.*, arXiv:hep-ph/0210192.
- [10] Workshop on “Radioactive beams for nuclear physics and neutrino physics”  
37<sup>th</sup> Rencontre de Moriond, Les Arcs (France) March 17-22nd, 2003;  
<http://moriond.in2p3.fr/radio/index.html>.

- [11] J. Burguet-Castell, D. Casper, J. J. Gomez-Cadenas, P. Hernandez and F. Sanchez, arXiv:hep-ph/0312068.
- [12] F. Terranova, A. Marotta, P. Migliozi and M. Spinetti, arXiv:hep-ph/0405081.
- [13] J. Bouchez, M. Lindroos and M. Mezzetto, arXiv:hep-ex/0310059.
- [14] J. J. Gomez-Cadenas *et al.* [CERN working group on Super Beams Collaboration], arXiv:hep-ph/0105297.
- [15] H. Minakata and H. Nunokawa, Phys. Lett. B **495** (2000) 369 [arXiv:hep-ph/0004114];  
V. D. Barger, S. Geer, R. Raja and K. Whisnant, Phys. Rev. D **63** (2001) 113011 [arXiv:hep-ph/0012017];  
V. D. Barger *et al.*, arXiv:hep-ph/0103052;  
H. Minakata and H. Nunokawa, JHEP **0110** (2001) 001 [arXiv:hep-ph/0108085];  
P. Huber, M. Lindner and W. Winter, Nucl. Phys. B **645** (2002) 3 [arXiv:hep-ph/0204352];  
G. Barenboim *et al.*, arXiv:hep-ex/0206025.
- [16] J. Burguet-Castell, M. B. Gavela, J. J. Gomez-Cadenas, P. Hernandez and O. Mena, Nucl. Phys. B **608** (2001) 301 [arXiv:hep-ph/0103258];  
J. Burguet-Castell and O. Mena, arXiv:hep-ph/0108109.
- [17] H. Minakata and H. Nunokawa, JHEP **0110** (2001) 001 [arXiv:hep-ph/0108085].
- [18] G. L. Fogli and E. Lisi, Phys. Rev. D **54** (1996) 3667 [arXiv:hep-ph/9604415].
- [19] V. Barger, D. Marfatia and K. Whisnant, Phys. Rev. D **65** (2002) 073023 [arXiv:hep-ph/0112119].
- [20] A. Donini, D. Meloni and S. Rigolin, arXiv:hep-ph/0312072.
- [21] C. K. Jung, arXiv:hep-ex/0005046.
- [22] P. Zucchelli, Phys. Lett. B **532** (2002) 166.
- [23] A. Cervera, A. Donini, M. B. Gavela, J. J. Gomez Cadenas, P. Hernandez, O. Mena and S. Rigolin, Nucl. Phys. B **579** (2000) 17 [Erratum-ibid. B **593** (2001) 731] [arXiv:hep-ph/0002108].
- [24] L.P. Ekström and R.B. Firestone, WWW Table of Radioactive Isotopes, from <http://ie.lbl.gov/toi/index.htm>
- [25] S. Gilardoni, to be published as CERN Thesis.  
S. Gilardoni, G. Grawer, G. Maire, J. M. Maugain, S. Rangod and F. Voelker, J. Phys. G **29** (2003) 1801.

- [26] G. P. Zeller, arXiv:hep-ex/0312061.
- [27] D. Casper, Nucl. Phys. Proc. Suppl. **112** (2002) 161 [arXiv:hep-ph/0208030].
- [28] J. Serreau and C. Volpe, arXiv:hep-ph/0403293.
- [29] P. Lipari, private communication;  
P. Lipari, M. Lusignoli and F. Sartogo, Phys. Rev. Lett. **74**, 4384 (1995)  
[arXiv:hep-ph/9411341].
- [30] M. Mezzetto, J. Phys. G **29** (2003) 1781 [arXiv:hep-ex/0302005].
- [31] Y. Itow *et al.*, arXiv:hep-ex/0106019.
- [32] A. Donini, D. Meloni and P. Migliozzi, Nucl. Phys. B **646** (2002) 321  
[arXiv:hep-ph/0206034];  
D. Autiero *et al.*, Eur. Phys. J. C **33** (2004) 243 [arXiv:hep-ph/0305185].

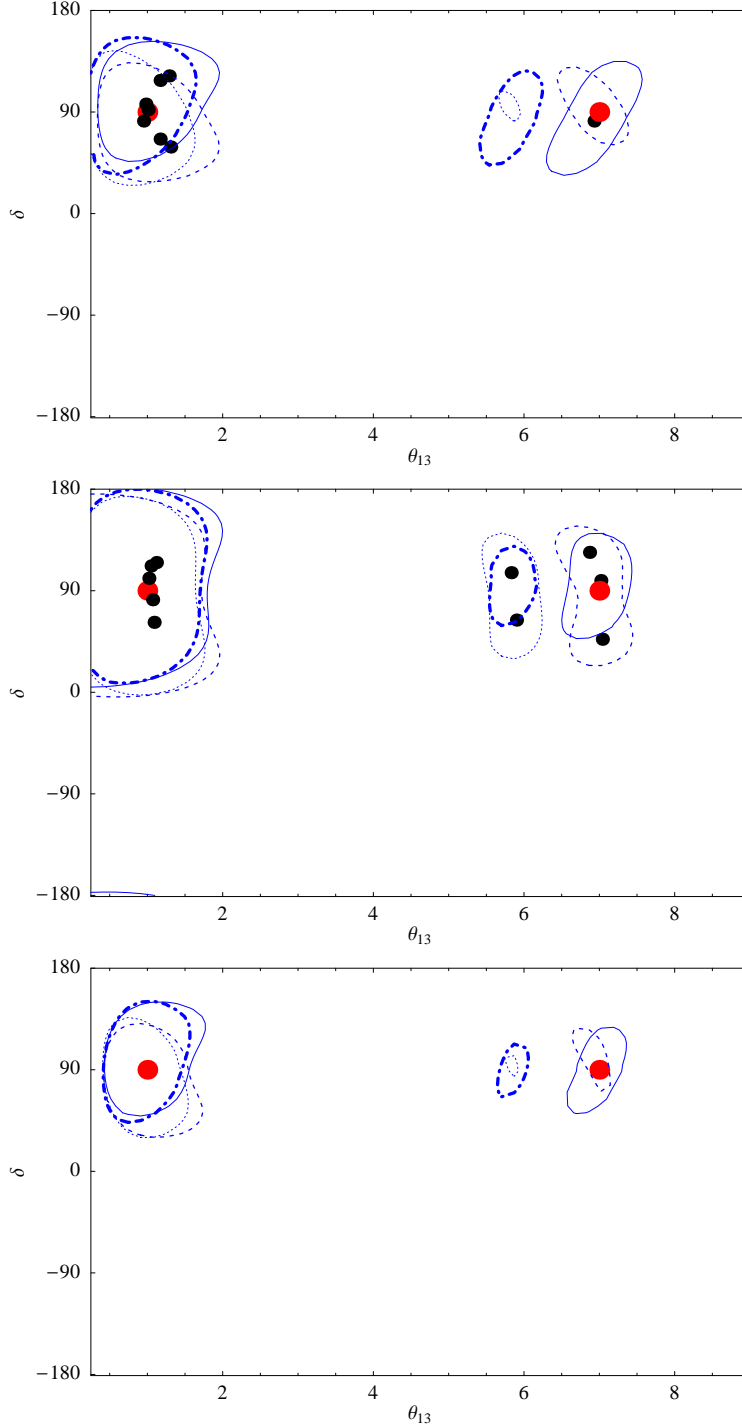


Figure 5: Fits to  $\theta_{13}$  and  $\delta$  after a 10 yrs  $\beta$ -Beam run and a 2+8 Super-Beam run. The 90% CL contours are shown for the following input values:  $\theta_{13} = 1^\circ, 7^\circ$  and  $\delta = 90^\circ$ . Upper panel:  $\beta$ -Beam results; middle panel: Super-Beam results; lower panel combined results. Continuous lines stand for the intrinsic degeneracy; dashed lines stand for the sign degeneracy; dot-dashed lines stand for the octant degeneracy; dotted lines stand for the mixed degeneracy. The light circle (red) shows the input value. Dark (black) dots are the theoretical clone locations computed as in Ref. [20].

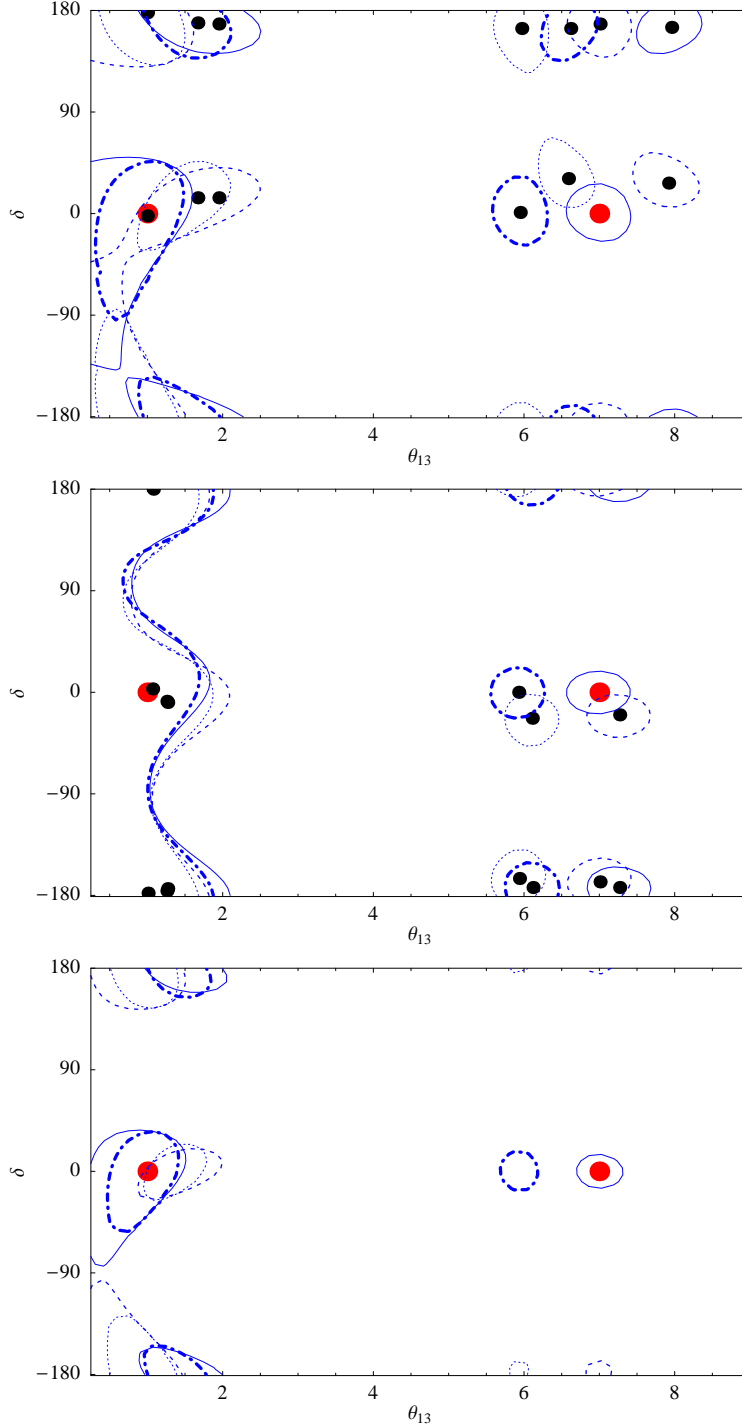


Figure 6: Fits to  $\theta_{13}$  and  $\delta$  after a 10 yrs  $\beta$ -Beam run and a 2+8 Super-Beam run. The 90% CL contours are shown for the following input values:  $\theta_{13} = 1^\circ, 7^\circ$  and  $\delta = 0$ . Upper panel:  $\beta$ -Beam results; middle panel: Super-Beam results; lower panel: combined results. Continuous lines stand for the intrinsic degeneracy; dashed lines stand for the sign degeneracy; dot-dashed lines stand for the octant degeneracy; dotted lines stand for the mixed degeneracy. The light circle (red) shows the input value. Dark (black) dots are the theoretical clone locations computed as in Ref. [20].

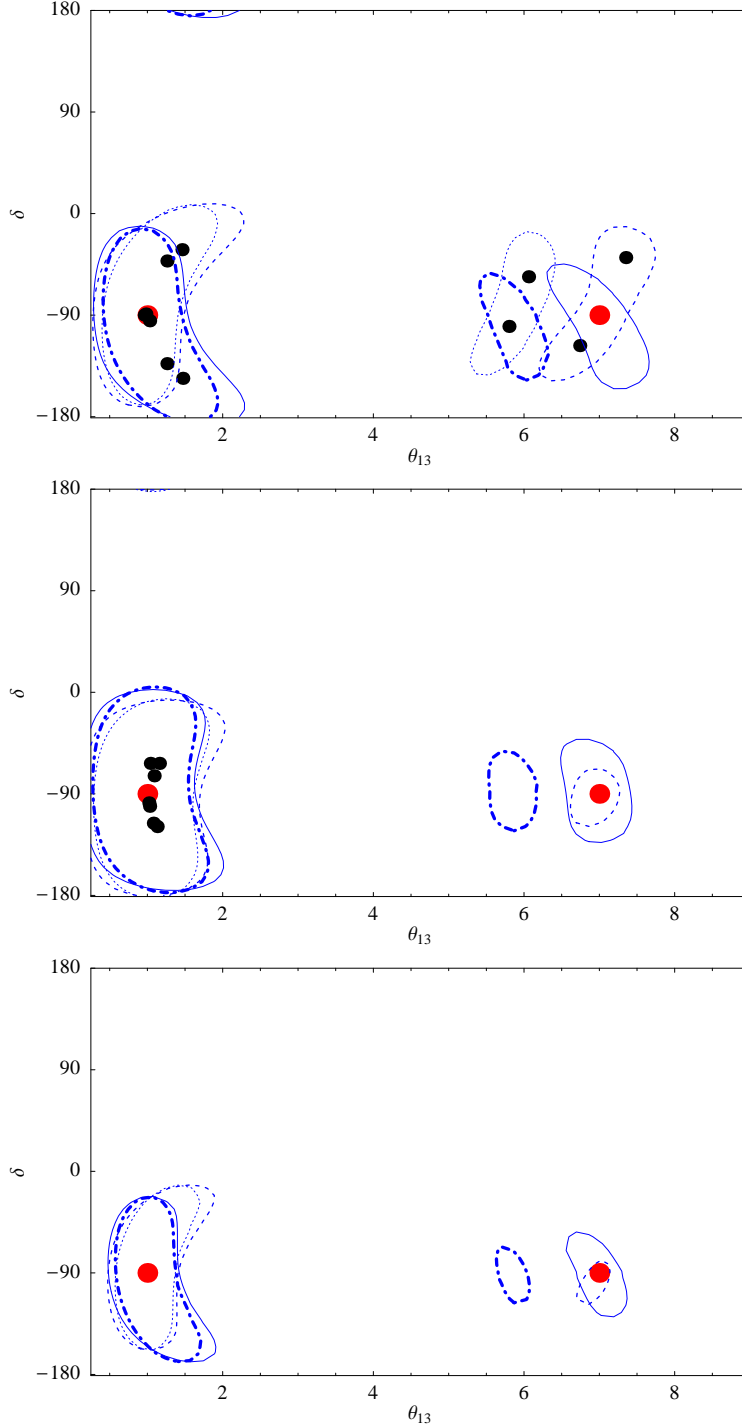


Figure 7: Fits to  $\theta_{13}$  and  $\delta$  after a 10 yrs  $\beta$ -Beam run and a 2+8 Super-Beam run. The 90% CL contours are shown for the following input values:  $\theta_{13} = 1^\circ, 7^\circ$  and  $\delta = -90^\circ$ . Upper panel:  $\beta$ -Beam results; middle panel: Super-Beam results; lower panel: combined results. Continuous lines stand for the intrinsic degeneracy; dashed lines stand for the sign degeneracy; dot-dashed lines stand for the octant degeneracy; dotted lines stand for the mixed degeneracy. The light circle (red) shows the input value. Dark (black) dots are the theoretical clone locations computed as in Ref. [20].

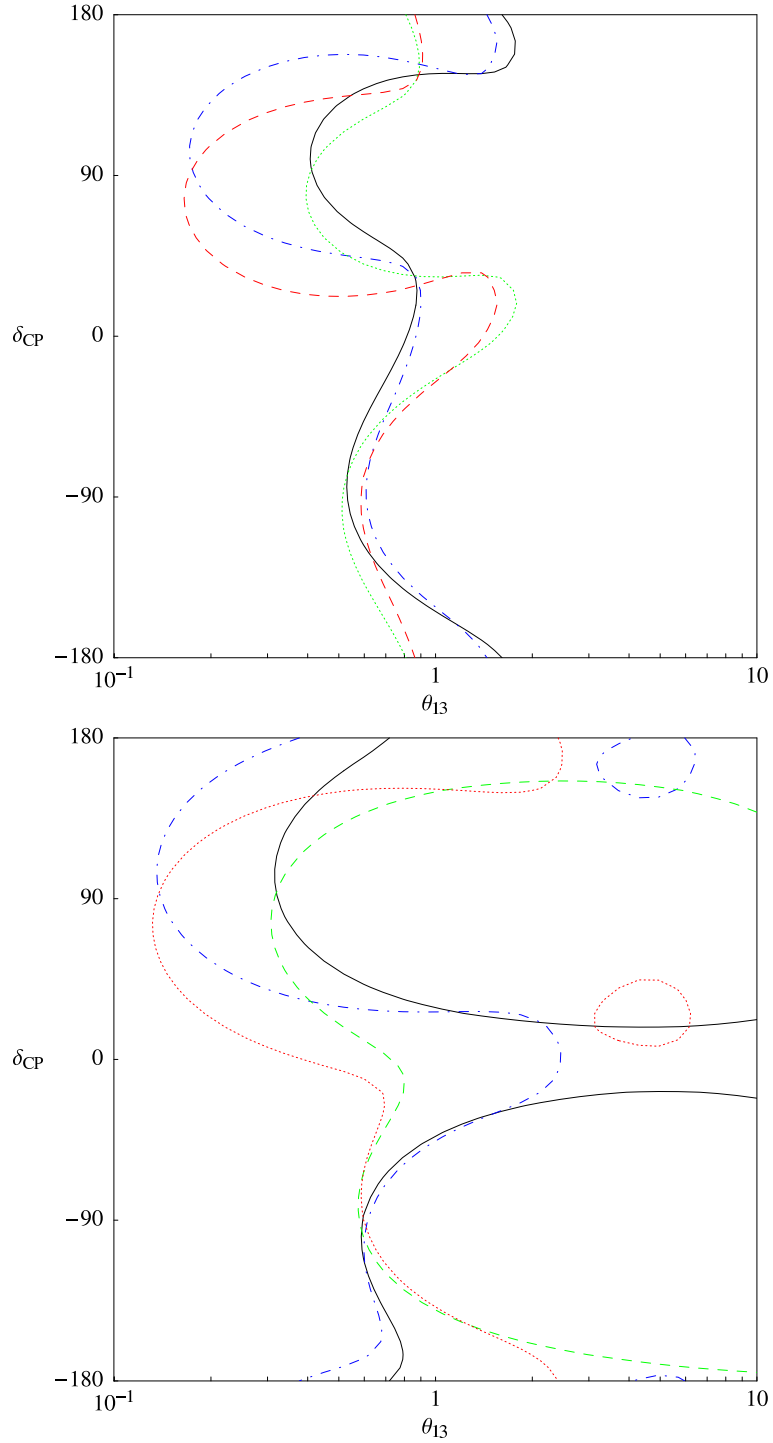


Figure 8: Sensitivity plots to  $\theta_{13}$  (upper) and  $\delta$  (lower) after a 10 yrs  $\beta$ -Beam run. The 90% CL contours are shown. Continuous lines stand for the intrinsic degeneracy; dashed lines stand for the sign degeneracy; dot-dashed lines stand for the octant degeneracy; dotted lines stand for the mixed degeneracy.

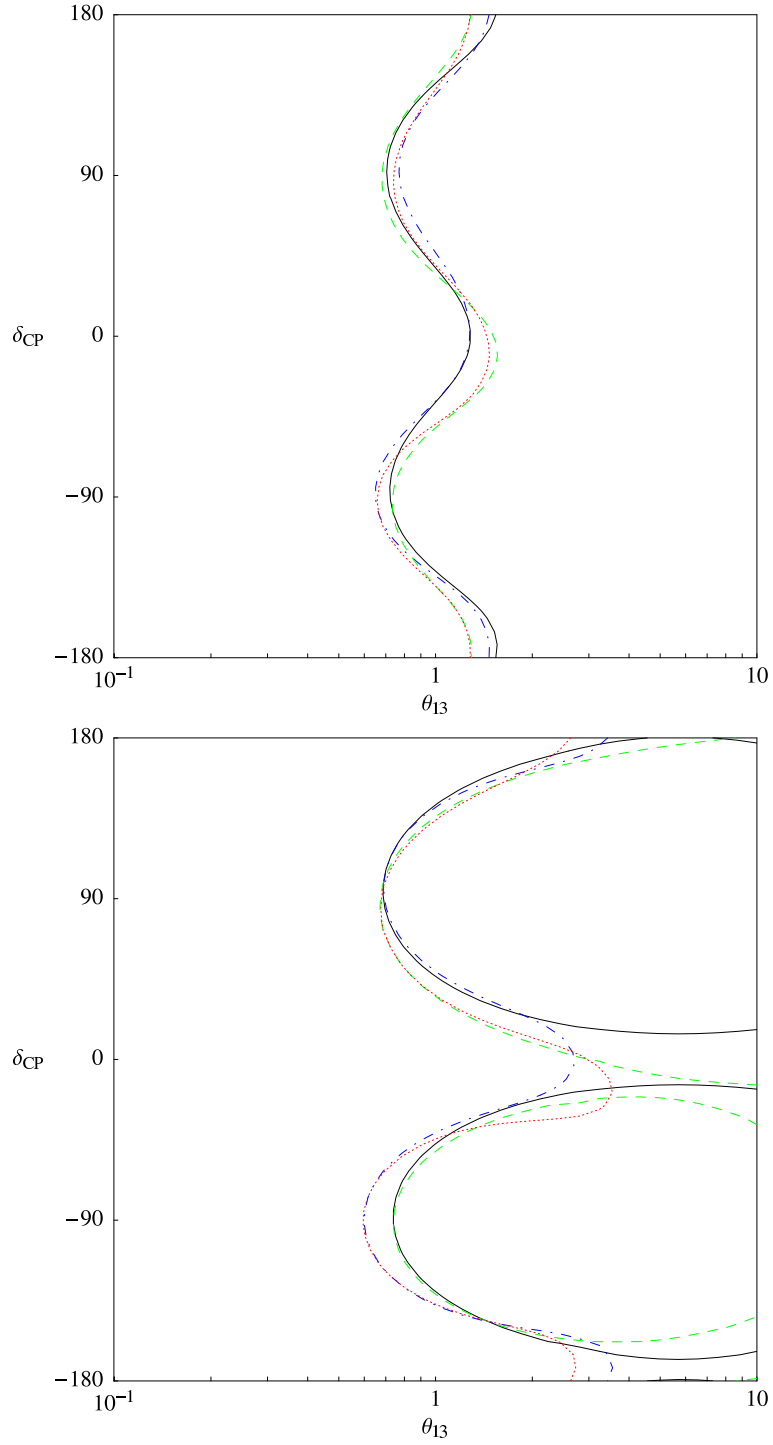


Figure 9: Sensitivity plots to  $\theta_{13}$  (upper) and  $\delta$  (lower) after a 2+8 Super-Beam run. The 90% CL contours are shown. Continuous lines stand for the intrinsic degeneracy; dashed lines stand for the sign degeneracy; dot-dashed lines stand for the octant degeneracy; dotted lines stand for the mixed degeneracy.



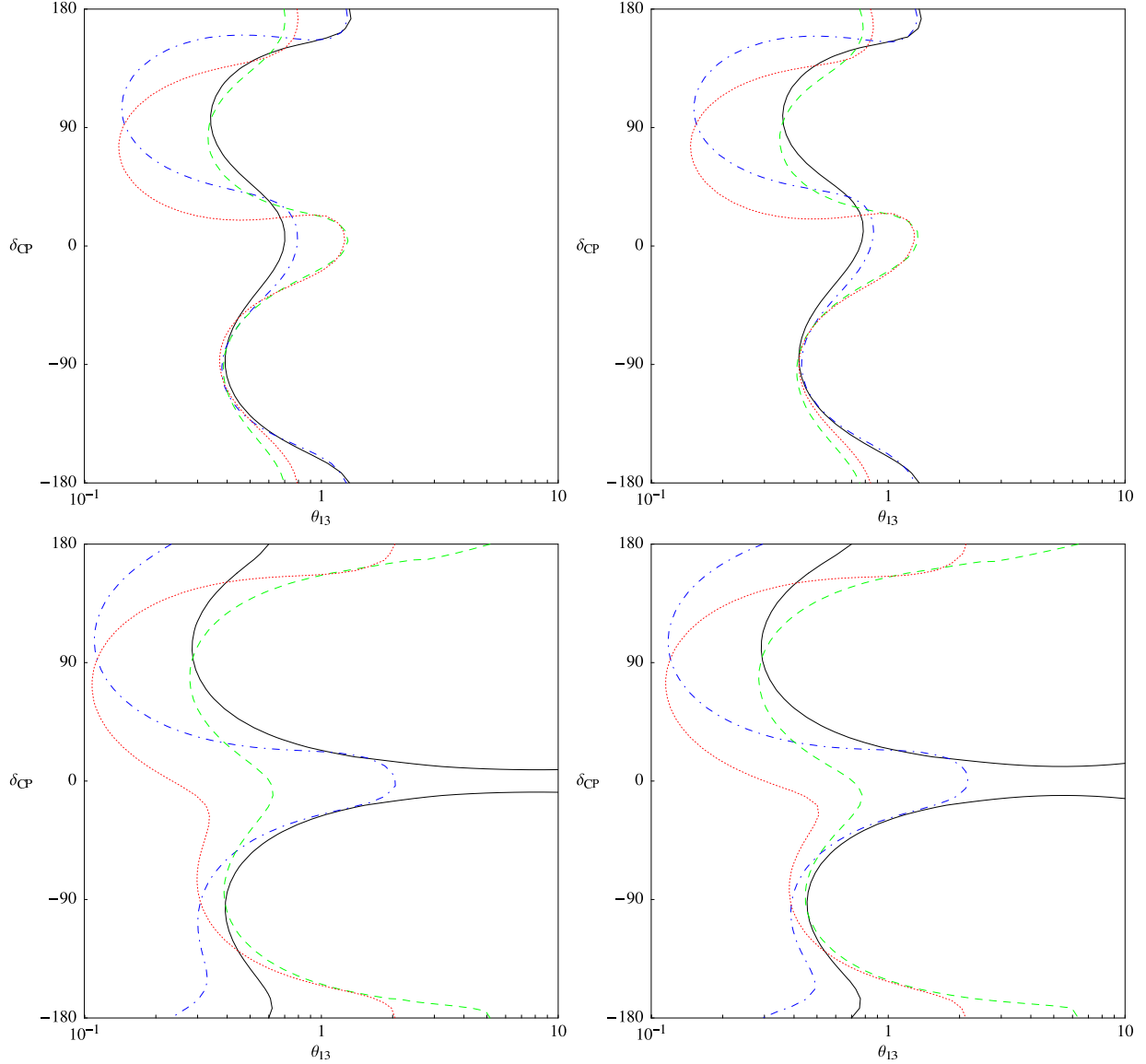


Figure 10: *Sensitivity plots to  $\theta_{13}$  (upper) and  $\delta$  (lower) after a combined 10 yrs  $\beta$ -Beam and a 2+8 Super-Beam run. The 90% CL contours for two values of the systematic errors are shown: 2% (left panels) and 5% (right panels). Continuous lines stand for the intrinsic degeneracy; dashed lines stand for the sign degeneracy; dot-dashed lines stand for the octant degeneracy; dotted lines stand for the mixed degeneracy.*